ACS Photonics

Article

Cite This: ACS Photonics XXXX, XXX, XXX−XXX

pubs.acs.org/journal/apchd5

# Complete Control of Smith-Purcell Radiation by Graphene Metasurfaces

Zhaoxian Su,[†] Feng Cheng,[‡] Lin Li,[†] and Yongmin Liu*[,†,‡]

[†]Department of Mechanical and Industrial Engineering and [‡]Department of Electrical and Computer Engineering, Northeastern University, Boston, Massachusetts 02115, United States

Supporting Information

**ABSTRACT:** Smith-Purcell radiation results from charged particles that move closely to a periodic structure. In this work, we report the on-demand control of Smith-Purcell radiation by rationally designed graphene metasurfaces. Not only can we strongly enhance the efficiency of Smith-Purcell radiation, but also the amplitude, phase, and polarization state of the radiated wave can be fully manipulated by tuning the structure and Fermi level of the graphene metasurface. Through designing the geometric parameters of each unit cell of the metasurface, the intensity of the radiated wave from each unit cell can be changed from zero to maximum. Meanwhile, the phase of the radiated wave at any position of the metasurface can change within a range of $2\pi$ by adjusting the displacement of the patterned graphene structures. Utilizing these two properties, we demonstrate that we can steer the direction of the Smith-Purcell radiation and focus the radiated wave with dual focal points. Furthermore, a circularly polarized wave with an arbitrary phase can also be realized via introducing cross-polarization. Our findings provide a new way to design electron-beam-induced light sources as well as particle detectors with high efficiency and a compact footprint.

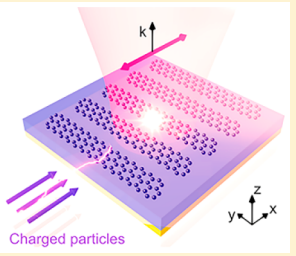


**KEYWORDS:** *Smith-Purcell radiation, metasurface, graphene, polarization*



As the two-dimensional (2D) equivalent of metamaterials, metasurfaces have become a very important area in nanophotonics, because they offer a new strategy to implement highly compact, planar optical devices.[1−4] Different from conventional optical devices that typically require phase accumulation in a bulk material, metasurfaces can realize a prescribed local phase and polarization within a 2D plane, thanks to the strong interaction between light and engineered subwavelength building blocks. Meanwhile, metasurfaces are relatively easier to fabricate and have lower losses compared to bulk metamaterials. Many kinds of metasurfaces, which can work from the optical to microwave regions, have been designed and fabricated to achieve different functions, such as beam steering,[5−7] focusing,[8−10] total absorption,[11−14] holograms,[15−17] and so on.

Recently, some efforts have been devoted to employing metamaterials to investigate the intriguing interaction among electrons, photons, and structured matter. This interaction could lead to electron-beam-induced emission over a broad wavelength range, which shows great potential applications in nanoscale light sources.[18−20] For example, reversed Cerenkov radiation has been proposed and observed in metamaterials.[21−24] Similarly, there has been a resurgence of interest in Smith-Purcell radiation mediated by metamaterials or metasurfaces.[25−30] Smith-Purcell radiation describes the light emission process when charged particles move closely and parallel to a periodic structure, with the velocity slower than the phase velocity of light in the surrounding medium.[31] Smith-Purcell radiation could be explained by the coupling between the evanescent fields of the moving charged particles and the electromagnetic modes of a periodic structure.[32] As a result, the Smith-Purcell effect strongly depends on the physical structure of the building blocks, providing us with an opportunity to manipulate the radiated light by structural designs. Recently, C-aperture Babinet metasurfaces have been proposed to control the polarization direction of Smith-Purcell radiation through induced cross-coupled electric and magnetic dipoles.[25] However, how to completely control other degrees of freedom, such as the phase and amplitude, of the radiated light, especially in a dynamically tunable manner, remains largely unexplored.

In the paper, we propose a graphene metasurface that consists of patterned graphene structures, including ribbons and patches, to fully control Smith-Purcell radiation. Graphene, a 2D material made of a monolayer of carbon atoms,[33] has attracted extensive interest in the design of metasurfaces due to its unique optical and electronic properties.[34−40] Doped graphene not only supports plasmonic excitations in the terahertz regime, but also shows an enhanced photonic density of states.[41] Recently, Wu et al. demonstrated that nonlinear graphene plasmons can be greatly enhanced through phase-match coupling.[42] By tuning the surface plasmon (SP) resonance of graphene patterns, we show that the phase, amplitude, and polarization states of the Smith-Purcell radiation can be controlled on demand. Using nonperfectly matched diffraction processes,[43,44] we numerically demonstrate that the phase of Smith-Purcell radiation can be tuned by changing the position of graphene ribbons. Meanwhile, the radiation amplitude, which is proportional to the strength of

**Received:** February 12, 2019
**Published:** July 5, 2019




DOI: 10.1021/acsphotonics.9b00251
ACS Photonics XXXX, XXX, XXX−XXX

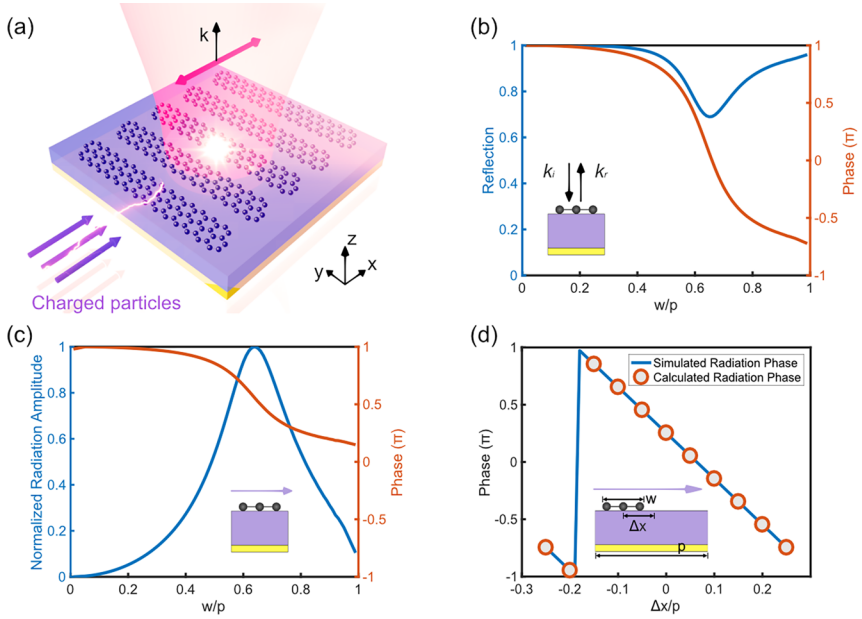


**Figure 1.** (a) Schematic of Smith-Purcell radiation mediated by graphene metasurfaces. (b) Dependence of the reflectance and phase on the width of the graphene ribbons when TM polarized light is normally incident on a metasurface consisting of periodic graphene ribbons. (c) Normalized radiation amplitude and phase of Smith-Purcell radiation induced by the same metasurface in (b). (d) Dependence of the radiation phase on the displacement of a graphene ribbon in its unit cell for the second-order Smith-Purcell radiation. In all the simulations, the Fermi level of the graphene ribbons is 0.48 eV and the frequency is 2 THz.

the SP resonance, can be manipulated by changing the width of the graphene ribbons. Leveraging these properties, we design two graphene metasurfaces, which can steer the direction of the Smith-Purcell radiation and focus the radiated wave, respectively. Finally, we extend the building block of the graphene metasurface from ribbons to patches. It is shown that a cross-polarized radiated wave can be excited when we adjust the orientation of the graphene patch. This allows us to achieve circularly polarized radiated waves by combing two graphene patches into a unit cell. The full control of Smith-Purcell radiation presented in this work manifests many potential applications in tunable light sources, on-chip particle detectors, holograms, and other novel optoelectronic devices.

The schematic of the Smith-Purcell radiation generated by a graphene metasurface is shown in Figure 1a. The graphene metasurface consists of patterned graphene structures (e.g., graphene ribbons), a dielectric spacing layer, and a thick metal film at the bottom serving as a perfect reflector to eliminate transmission. The thickness of the dielectric layer is $h = 15\ \mu$m. A uniform sheet of charged particles moves with a velocity of $v_0$ in the plane of $z = z_0 = 5\ \mu$m, while the graphene ribbons are in the plane of $z = 0$. The current density can be expressed as $\bar{J}(x, z, t) = \hat{x}qv_0\delta(z - z_0)\delta(x - v_0t)$, where $q$ is the charge density distribution per unit length in the $y$-direction, and $v_0$ is the velocity of moving charged particles. After Fourier transform, the current density in the frequency domain is then given by[25]

$$\bar{J}(x, z, \omega) = \frac{1}{2\pi}\int dt\bar{J}(x, z, t)e^{i\omega t} = \hat{x}I_0\delta(z - z_0)e^{ik_x x} \tag{1}$$

where $k_x = \omega/v_0$ and $I_0 = q/2\pi$. It should be noted that we use a 2D sheet of moving electrons, which is invariant along the $y$-axis, in order to simplify the simulation. In realistic experiments, an electron beam can be used to induce evanescent waves to interact with graphene metasurfaces. As indicated by a recent work,[45] a simplified 2D electron source could capture all the necessary physics involved in this process, because all the resonant modes of patterned graphene structures are transverse magnetic polarized. When the velocity of charged particles ($v_0$) is smaller than the phase velocity of light ($c$) in the surrounding medium, Smith-Purcell radiation can be generated due to the coupling between the evanescent fields associated with the moving charged particles and the periodic structure next to them. In this case, the evanescent fields induced by the surface current in the region $0 < z < z_0$ can be written as

$$\begin{cases} \bar{E}_i = -(\hat{x}i\gamma + \hat{z}k_x)\dfrac{I_0}{2\omega\varepsilon_0}e^{\gamma(z-z_0)+ik_x x} \\ \bar{H}_i = \hat{y}\dfrac{I_0}{2}e^{\gamma(z-z_0)+ik_x x} \end{cases} \tag{2}$$

where $\gamma = \sqrt{k_x^2 - k_0^2}$ and $\varepsilon_0$ is the vacuum permittivity. Equation 2 indicates that the field is transverse magnetic (TM) polarized. The reflected fields above the metasurface can be expanded in terms of Floquet modes:

$$\bar{H}_r = \sum_{m,n}\bar{H}_{mn}e^{i(k_x+mG)x+ik_{zm}z} \tag{3}$$

where $G = 2\pi/p$ is the Bloch wavevector associated with the periodicity $p$ along the $x$-direction, and $k_{zm} = \sqrt{k_0^2 - (k_x + mG)^2}$ is the wavenumber along the $z$-direction. To generate far-field radiation, we need $k_0^2 \geq (k_x + mG)^2$, which leads to a negative $m$ and a subwavelength periodicity $p$ (i.e., $p$ is smaller than the free-space wavelength $\lambda_0$). Consequently, the radiation wavelength and the periodicity should satisfy the relation:


DOI: 10.1021/acsphotonics.9b00251
ACS Photonics XXXX, XXX, XXX−XXX

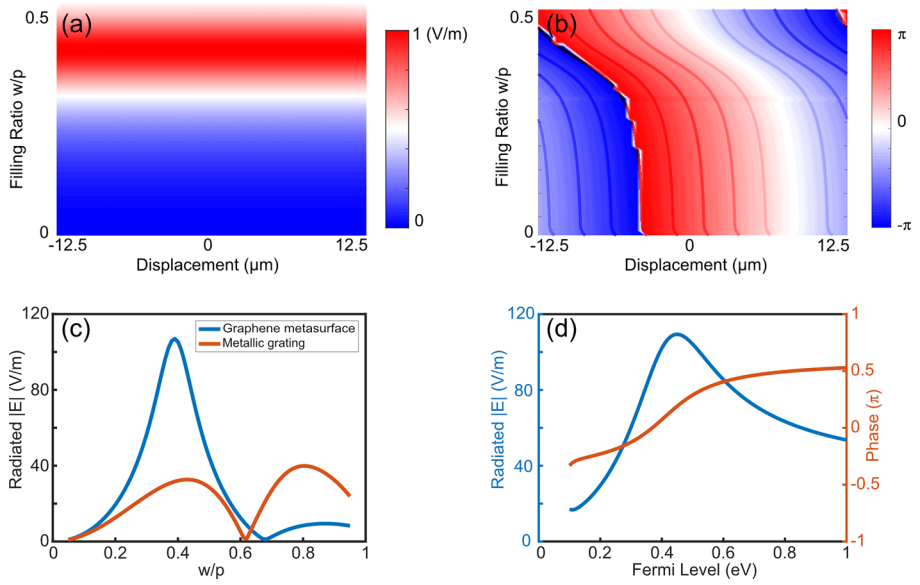


**Figure 2.** (a) Normalized radiation amplitude and (b) radiation phase with different filling ratios (defined as the ratio of ribbon width and period) and displacements of graphene ribbons. The contour lines in (b) are plotted according to eq 6. (c) Amplitude of radiation versus the width of the graphene ribbons or metallic grating. Here the graphene ribbon or metallic gratings is placed at the center of each unit cell (i.e., the displacement is 0). (d) Dependence of radiation amplitude and phase on the Fermi level of graphene. The frequency is 2 THz in all the simulations.

$$\left|\frac{\lambda_0 m}{p} + \frac{c}{v_0}\right| \leq 1, \quad \text{with} \quad m \leq -1 \tag{4}$$

When eq 4 is satisfied, the angle $\theta$ between the direction of the radiation wave and the moving particle can be defined as $\cos\theta = (k_x + mG)/k_0$. Hence, the relation between the wavelength and the radiation angle of Smith-Purcell radiation is given by

$$\lambda_0 = \frac{p}{|m|}\left(\frac{c}{v_0} - \cos\theta\right) \tag{5}$$

From eq 5 it is clear that the radiated light is along the $z$-axis at the radiation wavelength $\lambda_0 = pc/|m|v_0$.

We first investigate how to control the phase of Smith-Purcell radiation by a graphene metasurface consisting of graphene ribbons. In our design, we consider that the period of the metasurface is $p = 25\ \mu$m, and the frequency of radiated waves is $f = 2$ THz. The conductivity of graphene is described as the Kubo formula[46] and the scattering time $\tau = 1 \times 10^{-12}$ is assumed.[47] The Fermi level of the graphene ribbons is set as $E_f = 0.48$ eV. Here we consider nearly ideal graphene, while graphene grown by chemical vapor deposition (CVD) can also support pronounced SP resonances.[48,49] We discuss the results with practically achievable graphene parameters in the Supporting Information, which show similar effects presented in the main text. When the graphen metasurface is illuminated by a perpendicularly incident TM beam with electric field polarized along the $x$-axis, the strong SP resonance of the graphene ribbons can be excited. The dielectric spacing layer and the metallic back reflector form an optical cavity, which can enhance the interaction between incident light and graphene surface plasmons.[50−52] Consequently, the phase modulation range could reach $2\pi$ with the variation of the width of graphene ribbons, as shown in Figure 1b. In this case, the reflected fields of the metasurface can be regarded as the interference of the radiated fields from the resonant structure and the direct reflected fields from the metal mirror at the bottom. However, the situation is different for Smith-Purcell radiation, because the graphene ribbons are excited by TM polarized evanescent fields associated with the moving charged particles. The far-field radiation results from the coupling of evanescent fields and subwavelength resonant structures. Only the radiated fields with higher Floquet modes from the resonant structure itself can propagate to the far field. It turns out that the phase modulation range of the Smith-Purcell radiation limits to $\pi$ when varying the width of the graphene ribbons (Figure 1c), due to the lack of the interference with the direct reflection in the far field. Therefore, we need a new strategy to achieve the phase modulation range of $2\pi$, which is the key to control the radiation.

One approach is to utilize displacement-dependent phase modulation as described in the following. When the graphene ribbon shifts from the center of the unit cell with a displacement $\Delta x$, the effective conductivity of the graphene metasurface in the $xy$-plane can be expressed as $\sigma_{\text{eff}} = \sum_m \sigma_m e^{imG\cdot(x+\Delta x)}$. Excited by the incident fields of the charged particles, the effective current of the metasurface $J = \sigma_{\text{eff}} E_i$ can be regarded as the source of the Smith-Purcell radiation. Due to the momentum conservation, the Smith-Purcell radiation added an extra phase $mG\Delta x$. As a result, the phase of Smith-Purcell radiation follows:

$$\varphi = \varphi_0 + mG\Delta x, \quad \text{with} \quad -p/2 < \Delta x < p/2 \tag{6}$$

Here, $\phi_0$ is the phase of radiated light when the graphene ribbon is at the center of its unit cell (i.e., $\Delta x = 0$). In the case of $m = -1$ (i.e., first-order Floquet mode), the phase modulation range of the radiated light can reach $2\pi$ when $\Delta x$ changes from $-p/2$ to $p/2$. Considering the finite width of graphene ribbons with respect to the period, we take $m = -2$ (i.e., second-order Floquet mode), in which case the phase modulation range of the radiated light can reach $2\pi$, with $\Delta x$ changing from $-p/4$ to $p/4$. We have simulated the radiation wave at 2 THz, when the period of the graphene metasurface is increased to $p = 50\ \mu$m and the velocity of charged particles is $v_0 = c/6$. The dependence of phase on the displacement, $\Delta x$, is shown in Figure 1d. We have also used eq 5 to calculate the radiation phase, which agrees perfectly with the simulated values. Hence, the phase of the Smith-Purcell



DOI: 10.1021/acsphotonics.9b00251
ACS Photonics XXXX, XXX, XXX−XXX

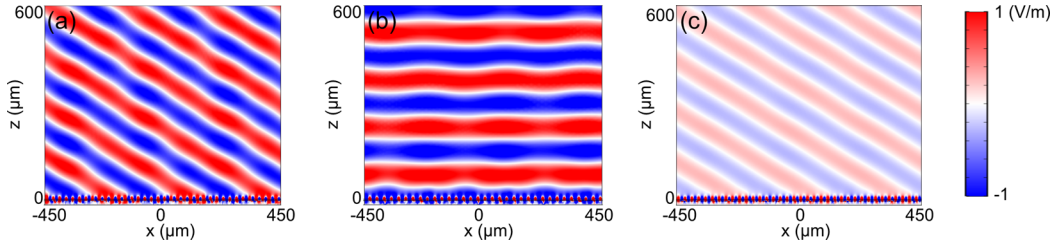


**Figure 3.** Electric field distribution of Smith-Purcell radiation generated by a graphene metasurface at a frequency of (a) 2 THz (a) and (b) 1.83 THz. The displacement-induced phase difference is $d\phi = \pi/3$ between adjacent unit cells. (c) Electric field distribution of Smith-Purcell radiation is 2 THz when the Fermi level of the graphene ribbons is changed from to 0.48 eV used in (a) and (b) to 0.24 eV.

radiation could be easily tuned from 0 to $2\pi$ by varying the displacement of the graphene ribbons in the unit cell.

The amplitude of Smith-Purcell radiation can be controlled and enhanced, owing to the strong plasmon resonance of graphene ribbons that depends on the width of ribbons.[53−57] SP resonances of graphene ribbons can be excited by the evanescent fields when the wavevector of graphene surface plasmon $k_{spp}$ satisfies the phase matching condition $k_{spp} = k_x$. In our design, the incident fields are evanescent fields with a large value of $k_x$. The SP resonance of the graphene ribbons can be excited without adding an additional Bloch wavevector. The radiation amplitude will be enhanced, thanks to the electric field enhancement of graphene SP resonance. Thus, we can control the amplitude of Smith-Purcell radiation by varying the width of the graphene ribbons. Figure 2a presents the simulation result of the radiation amplitude of the metasurface at 2 THz with different filling ratios of graphene ribbons (defined as the ratio of ribbon width and periodicity) and different displacements. Here, the Fermi level of the graphene ribbons is set as $E_f = 0.48$ eV. We find that the radiation amplitude varies rapidly with the ribbon width. However, the radiation amplitude is insensitive to the displacement of graphene ribbons because the SP resonance of the graphene ribbon does not rely on its position. On the contrary, the phase modulation, as shown in Figure 2b, has weak dependence on the filling ratio, except when the filling ratio is around 0.4, which induces the graphene SP resonance at 2 THz. By changing the displacement of graphene ribbons, we can tune the phase of the radiated light from 0 to $2\pi$, regardless of the amplitude of the graphene SP resonance. The results in Figure 2a,b show that the radiation amplitude and phase can be controlled via different physical mechanisms, which provide us with independent degrees of freedom to tailor the radiated light.

In addition to the full control of the radiated wave, high radiation efficiency is another advantage of graphene metasurface. We have compared the radiation efficiency of the graphene metasurface with that of the traditional one-dimensional metallic grating. The result is shown in the Figure 2c. In the simulation, the periodicity of both the metallic grating and graphene metasurface is set as $p = 50$ $\mu$m. We choose gold with a conductivity of $4 \times 10^7$ S/m to construct the metallic grating, and its thickness is set as 0.2 $\mu$m. Because of the superior field confinement and enhancement of graphene plasmons at terahertz, the coupling efficiency between the evanescent fields and the SP resonance of graphene ribbons is much higher than the case when a metallic grating is used. As a result, the Smith-Purcell radiation induced by graphene metasuface can achieve higher radiation efficiency. Meanwhile, because the SP resonance of graphene ribbons has a dependence on the conductivity of graphene, which could be adjusted by changing the Fermi level via electrogating. We have simulated the radiation amplitude and phase induced by the graphene metasurface with a fixed width of $0.39p$ and different Fermi energies, as shown in Figure 2d. One can clearly see that the Smith-Purcell radiation can be adjusted by changing the Fermi level of graphene ribbons.

Since the phase of the radiated light can be tuned from 0 to $2\pi$, we can apply graphene metasurfaces to steer the radiated light by designing a proper phase gradient profile. Consider that the phase difference of the optical path of the radiation wave from two adjacent unit cells is zero:[2]

$$[(k_x - mG)dx + \varphi] - [k_0 \sin(\theta)dx + (\varphi + d\varphi)] = 0 \tag{7}$$

where $dx$ is the distance between the adjacent unit cells. The relation between the radiation angle and phase gradient is then given by

$$\sin\theta = \frac{c}{v_0} - \frac{m\lambda_0}{p} + \frac{\lambda_0}{2\pi}\frac{d\varphi}{dx} \tag{8}$$

Figure 3a shows the field distribution of the Smith-Purcell radiation at 2 THz when the metasurface has a constant in-plane phase difference between adjacent unit cells $d\phi = \pi/3$. At this frequency, the radiated light should propagate along the $z$-axis as charged particles move above a periodic structure according to the eq 4. However, using the proposed graphene metasurface with displaced graphene ribbons to implement the phase difference of $d\phi = \pi/3$, one can steer the direction of the radiated light to 30°. At another frequency, 1.83 THz, the radiated light, which should propagate at the direction of $\theta = -30°$ with a periodic structure, now propagates almost along the $z$-axis by using the same graphene metasurface (Figure 3b). We have also simulated the Smith-Purcell radiation when the Fermi level of graphene ribbons is varied, as shown in Figure 3c. Because the phase gradient does not change, the radiated light still propagates at 30°, but the radiated amplitude drops due to the change of Fermi level.

For practical applications, focusing Smith-Purcell radiation without any bulky lenses is of importance, which can also be obtained by designing the displacement of the graphene ribbon within the unit cells. Note that the amplitude and phase of the radiated light can be independently tuned by the graphene metasurface through the width and the displacement of graphene ribbons, respectively. It offers great convenience to design a focusing lens with multiple focal points. To make the radiated waves from the metasurface constructively interfere with each other at the focal points, not only the phase along the metasurface, but also the amplitude at the local point of the metasurface should be considered. Mathematically, the normalized complex amplitude along the metasurface can be expressed as



DOI: 10.1021/acsphotonics.9b00251
ACS Photonics XXXX, XXX, XXX−XXX

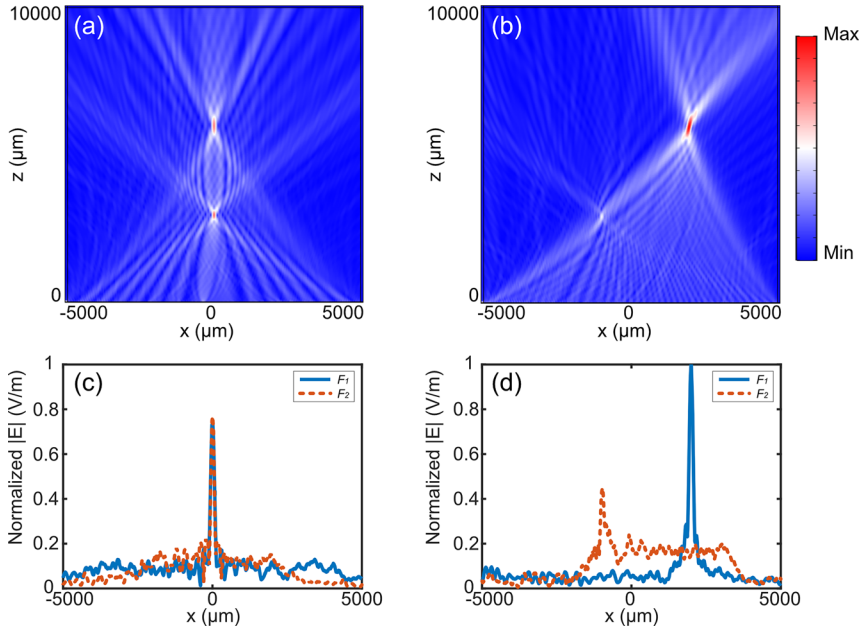


**Figure 4.** Distribution of normalized electric fields produced by a dual-focus graphene metalens with different design parameters. (a) Lateral locations of the two focal points are $x_1 = x_2 = 0$, and weight factors are $A_1 = A_2 = 0.5$. (b) Lateral locations of the two focal points are $x_1 = -1000$ $\mu$m and $x_2 = 2000$ $\mu$m, and weight factors are $A_1 = 0.3$ and $A_2 = 0.7$. (c) and (d) plot the normalized electric field amplitude across the focal points in (a) and (b), accordingly.

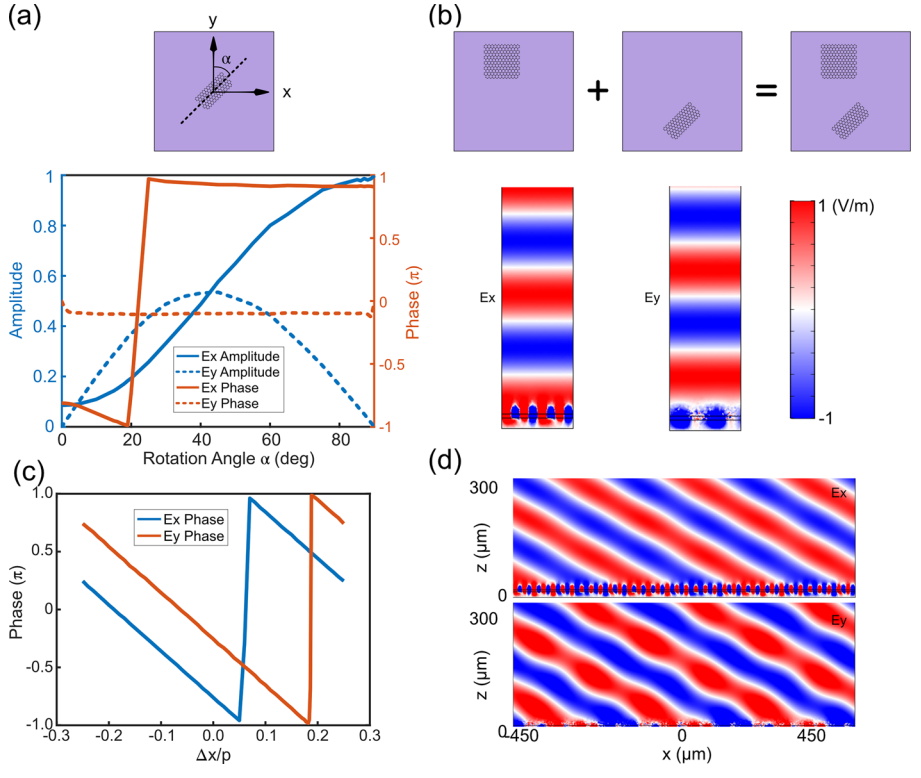


**Figure 5.** (a) Normalized radiation amplitude and phase of Smith-Purcell radiation induced by a metasurface that is composed of rotated rectangular graphene patches. (b) Distribution of $E_x$ and $E_y$ of the radiated wave induced by a graphene metasurface, whose unit cell has a rotated rectangular graphene patch and a square graphene patch. (c) The dependence of the phase of $E_x$ and $E_y$ components of the emitted light on the displacement of the combined graphene graphene patches. (d) Electric field distribution of $E_x$ and $E_y$ of circularly polarized Smith-Purcell radiation induced by the graphene metasurface with a phase difference of d$\phi = \pi/3$ between adjacent unit cells along the $x$-axis.

$$E(x) = \sum_{i=1}^{n} A_i \exp\left(i \cdot \frac{2\pi}{\lambda}\left(\sqrt{F_i^2 + (x - x_i)^2} - F_i\right)\right) \quad (8a)$$

Here $F_i$ is the focal length of the $i$th focal point, $x_i$ is the horizontal offset of the $i$th focal point from the central axis (that is, $x = 0$), $A_i$ is the weight factor to tune the relative amplitude of the $i$th focal point that satisfies $\sum_{i=1}^{n} A_i = 1$. As a proof-of-



DOI: 10.1021/acsphotonics.9b00251
ACS Photonics XXXX, XXX, XXX−XXX

principle demonstration, we consider a dual-focus metalens with a focal length of $F_1 = 40\lambda$ and $F_2 = 20\lambda$, respectively. Figure 4a shows the radiated field distribution without horizontal offset of the two focal points ($x_1 = x_2 = 0$), and the weight factors are identical ($A_1 = A_2 = 0.5$). Similarly, we have designed another metalens, as shown in Figure 4b, for which the two focal points are located at $x_1 = -1000$ $\mu$m and $x_2 = 2000$ $\mu$m, respectively, and the weight factors are different ($A_1 = 0.3$ and $A_2 = 0.7$). We can clearly see that the two focal points are at the designed positions. The details about the width of each graphene ribbon of the two metalenses is provided in the Supporting Information. To make a quantitative comparison, in Figure 4c and 4d we plot the electric field amplitude along a horizonal line across the focal points (i.e., $z = F_1$ and $z = F_2$). The amplitude of the electric fields at the focal points indeed matches the predesignated weight factors very well. The proposed graphene metalens shows the ability of focusing radiated wave at desired positions, which may lead to integrated, high-intensity light sources without any external bulky optical elements.

Finally, we will show that the polarization of Smith-Purcell radiation can be controlled as well. The radiated light generated by the metasurface based on graphene ribbons is always polarized along the $x$-axis, because the graphene plasmon resonances induce an array of electric dipoles oriented along the $x$-axis. To overcome this limitation and generate radiated field polarized along the $y$-axis, we need to induce electric dipoles pointing along the same direction, which can be realized by a rotated rectangular graphene patch. Figure 5a depicts the amplitude and phase of the radiated field in the $x$- and $y$-directions as a function of the rotation angle. In the simulation, the periodicity of the metasurface in the $x$- and $y$-directions is $p = 50$ $\mu$m and the width and length of the rotated graphene patch are $0.15p$ and $0.3p$, respectively. As shown in Figure 5a, in the case of $\alpha = 0$ and $\pi/2$, the amplitude of $E_y$ in the far field is nearly 0. Meanwhile, in the case of $\alpha \sim \pi/4$, the amplitude of $E_y$ equals $E_x$. If we want to generate a circularly polarized radiated wave, the amplitude of $E_x$ and $E_y$ should be equal and their phase difference should be $\pm\pi/2$. However, the phase difference between $E_y$ and $E_x$ is only $\pi$. Therefore, we resort to the proper phase difference by combining the rotated rectangular graphene patch of $\alpha = \pi/4$ with an additional square graphene patch in a unit cell. The coupling between the two graphene patches is weak, so that the phase and amplitude of radiated $E_y$ mainly result from rotation of the rotated rectangular graphene patch. By changing the geometry size and the horizontal displacement of the square graphene ribbon, we can tune the radiated field amplitude and phase from the square patch. Through the interference of the radiated field from the two patches, we can obtain equal amplitude of the $E_x$ and $E_y$ components in the emission and a phase difference of $\pm\pi/2$. Figure 5b shows the field distribution of $E_x$ and $E_y$ when a square graphene patch with a width of $0.3p$ and displacement of $\Delta x = -0.1p$ is added into the unit cell. From the field distribution, we can clearly see that the amplitudes of $E_x$ and $E_y$ are equal, and their phase difference is $\pi/2$, confirming that right circularly polarized light is generated. Because of the symmetry, the left circularly polarized wave can be readily realized with a rotation angle $\alpha = -\pi/4$ and a displacement of $\Delta x = 0.1p$. We can further control the propagation direction of the circularly polarized emission via proper phase gradient by changing the displacement of the combined two graphene patches, as we have discussed before. Figure 5c shows that the phase of $E_x$ and $E_y$ varies from $-\pi$ to $\pi$, when the displacement of the two combined graphene patches changes from $-p/4$ to $p/4$. By introducing a phase difference of $d\phi = \pi/3$ between adjacent unit cells along the $x$-axis, we can steer the radiated circularly polarized wave to 30°, as shown in Figure 5d.

In conclusion, we theoretically and numerically demonstrate the complete control of Smith-Purcell radiation by graphene metasurfaces. Through changing the displacement of graphene ribbons, we can add an additional phase to the radiated wave. As a result, the phase of the radiated wave can be tuned in the full range of $2\pi$. Meanwhile, we can control the amplitude of Smith-Purcell radiation by changing the width of graphene ribbons, because the width influences the strength of the induced graphene plasmon resonance. The cross-polarized radiation can be obtained via rotated graphene patches. Combining two graphene patches within a unit cell and properly adjusting their relative orientations and positions, we can generate circularly polarized Smith-Purcell radiation from the metasurface. The strategy presented here can be used to design electron-beam-induced light sources, holograms, and other novel electro-optical devices on the chip scale. It also sheds new light on the interactions between electrons, photons and structure light, which may help us to develop new techniques to probe material properties.

## ■ ASSOCIATED CONTENT

### Supporting Information

The Supporting Information is available free of charge on the ACS Publications website at DOI: 10.1021/acsphotonics.9b00251.

The description of the manipulation of Smith-Purcell radiation using CVD-grown graphene, and the geometric parameters of the focusing graphene metasurfaces (PDF)

## ■ AUTHOR INFORMATION


### Corresponding Author

*E-mail: y.liu@northeastern.edu.

### ORCID

Yongmin Liu: 0000-0003-1084-6651


### Notes

The authors declare no competing financial interest.

## ■ ACKNOWLEDGMENTS

We acknowledge the financial support from the Office of Naval Research (N00014-16-1-2409).

## ■ REFERENCES


(1) Yu, N.; Capasso, F. Flat optics with designer metasurfaces. *Nat. Mater.* **2014**, *13*, 139−150.

(2) Yu, N.; Genevet, P.; Kats, M. A.; Aieta, F.; Tetienne, J. P.; Capasso, F.; Gaburro, Z. Light propagation with phase discontinuities: generalized laws of reflection and refraction. *Science* **2011**, *334*, 333.

(3) Holloway, C. L.; Kuester, E. F.; Gordon, J. A.; O'Hara, J.; Booth, J.; Smith, D. R. An overview of the theory and applications of metasurfaces: The two-dimensional equivalents of metamaterials. *IEEE Antenn. Propag. M.* **2012**, *54*, 10.

(4) Kildishev, A. V.; Boltasseva, A.; Shalaev, V. M. Planar photonics with metasurfaces. *Science* **2013**, *339*, 1232009.

(5) Carrasco, E.; Tamagnone, M.; Mosig, J. R.; Low, T.; Perruisseau-Carrier, J. Gate-controlled mid-infrared light bending with aperiodic graphene nanoribbons array. *Nanotechnology* **2015**, *26*, 134002.

(6) Su, Z.; Chen, X.; Yin, J.; Zhao, X. Graphene-based terahertz metasurface with tunable spectrum splitting. *Opt. Lett.* **2016**, *41*, 3799−3802.




DOI: 10.1021/acsphotonics.9b00251
*ACS Photonics* XXXX, XXX, XXX−XXX

(7) Pfeiffer, C.; Emani, N. K.; Shaltout, A. M.; Boltasseva, A.; Shalaev, V. M.; Grbic, A. Efficient light bending with isotropic metamaterial huygens' surfaces. *Nano Lett.* **2014**, *14*, 2491.
(8) AbdollahRamezani, S.; Arik, K.; Khavasi, A.; Kavehvash, Z. Analog computing using graphene-based metalines. *Opt. Lett.* **2015**, *40*, 5239−42.
(9) Aieta, F.; Genevet, P.; Kats, M. A.; Yu, N.; Blanchard, R.; Gaburro, Z.; Capasso, F. Aberration-free ultrathin flat lenses and axicons at telecom wavelengths based on plasmonic metasurfaces. *Nano Lett.* **2012**, *12*, 4932.
(10) Yang, Q.; Gu, J.; Wang, D.; Zhang, X.; Tian, Z.; Ouyang, C.; Singh, R.; Han, J.; Zhang, W. Efficient flat metasurface lens for terahertz imaging. *Opt. Express* **2014**, *22*, 25931.
(11) Lobet, M.; Majerus, B.; Henrard, L.; Lambin, P. Perfect electromagnetic absorption using graphene and epsilon-near-zero metamaterials. *Phys. Rev. B: Condens. Matter Mater. Phys.* **2016**, *93*, 235424.
(12) Yao, Y.; Shankar, R.; Kats, M. A.; Song, Y.; Kong, J.; Loncar, M.; Capasso, F. Electrically Tunable Metasurface Perfect Absorbers for Ultrathin Mid-Infrared Optical Modulators. *Nano Lett.* **2014**, *14*, 6526−6532.
(13) Su, Z.; Yin, J.; Zhao, X. Terahertz dual-band metamaterial absorber based on graphene/MgF2 multilayer structures. *Opt. Express* **2015**, *23*, 1679−1690.
(14) Liu, X.; Fan, K.; Shadrivov, I. V.; Padilla, W. J. Experimental realization of a terahertz all-dielectric metasurface absorber. *Opt. Express* **2017**, *25*, 191−201.
(15) Zheng, G.; Muhlenbernd, H.; Kenney, M.; Li, G.; Zentgraf, T.; Zhang, S. Metasurface holograms reaching 80% efficiency. *Nat. Nanotechnol.* **2015**, *10*, 308−312.
(16) Ni, X.; Kildishev, A. V.; Shalaev, V. M. Metasurface holograms for visible light. *Nat. Commun.* **2013**, *4*, 2807.
(17) Wang, L.; Kruk, S.; Tang, H.; Li, T.; Kravchenko, I.; Neshev, D. N.; Kivshar, Y. S. Grayscale transparent metasurface holograms. *Optica* **2016**, *3*, 1504−1505.
(18) Su, Z.; Xiong, B.; Xu, Y.; Cai, Z.; Yin, J.; Peng, R.; Liu, Y. Manipulating Cherenkov Radiation and Smith−Purcell Radiation by Artificial Structures. *Adv. Opt. Mater.* **2019**, 1801666.
(19) Adamo, G.; MacDonald, K. F.; Fu, Y. H.; Wang, C. M.; Tsai, D. P.; Garcia de Abajo, F. J.; Zheludev, N. I. Light well: a tunable free-electron light source on a chip. *Phys. Rev. Lett.* **2009**, *103*, 113901.
(20) Adamo, G.; Ou, J. Y.; So, J. K.; Jenkins, S. D.; De Angelis, F.; MacDonald, K. F.; Di Fabrizio, E.; Ruostekoski, J.; Zheludev, N. I. Electron-beam-driven collective-mode metamaterial light source. *Phys. Rev. Lett.* **2012**, *109*, 217401.
(21) Veselago, V. G The electrodynamics of substances with simultaneously negative values of $\varepsilon$ and $\mu$. *Soviet Physics Uspekhi* **1968**, *10*, 509.
(22) Xi, S.; Chen, H.; Jiang, T.; Ran, L.; Huangfu, J.; Wu, B.-I.; Kong, J. A.; Chen, M. Experimental Verification of Reversed Cherenkov Radiation in Left-Handed Metamaterial. *Phys. Rev. Lett.* **2009**, *103*, 194801.
(23) Liu, S.; Zhang, P.; Liu, W.; Gong, S.; Zhong, R.; Zhang, Y.; Hu, M. Surface Polariton Cherenkov Light Radiation Source. *Phys. Rev. Lett.* **2012**, *109*, 153902.
(24) Vorobev, V. V.; Tyukhtin, A. V. Nondivergent Cherenkov Radiation in a Wire Metamaterial. *Phys. Rev. Lett.* **2012**, *108*, 184801.
(25) Wang, Z.; Yao, K.; Chen, M.; Chen, H.; Liu, Y. Manipulating Smith-Purcell Emission with Babinet Metasurfaces. *Phys. Rev. Lett.* **2016**, *117*, 157401.
(26) Yang, Y.; Massuda, A.; Roques-Carmes, C.; Kooi, S. E.; Christensen, T.; Johnson, S. G.; Joannopoulos, J. D.; Miller, O. D.; Kaminer, I.; Soljačić, M. Maximal spontaneous photon emission and energy loss from free electrons. *Nat. Phys.* **2018**, *14*, 894−899.
(27) Kaminer, I.; Kooi, S. E.; Shiloh, R.; Zhen, B.; Shen, Y.; López, J. J.; Remez, R.; Skirlo, S. A.; Yang, Y.; Joannopoulos, J. D.; Arie, A.; Soljačić, M. Spectrally and Spatially Resolved Smith-Purcell Radiation in Plasmonic Crystals with Short-Range Disorder. *Phys. Rev. X* **2017**, *7*, 011003.
(28) Liu, F.; Xiao, L.; Ye, Y.; Wang, M.; Cui, K.; Feng, X.; Zhang, W.; Huang, Y. Integrated Cherenkov radiation emitter eliminating the electron velocity threshold. *Nat. Photonics* **2017**, *11*, 289.
(29) Zhan, T.; Han, D.; Hu, X.; Liu, X.; Chui, S.-T.; Zi, J. Tunable terahertz radiation from graphene induced by moving electrons. *Phys. Rev. B: Condens. Matter Mater. Phys.* **2014**, *89*, 245434.
(30) Saavedra, J. R. M.; Castells-Graells, D.; García de Abajo, F. J. Smith-Purcell radiation emission in aperiodic arrays. *Phys. Rev. B: Condens. Matter Mater. Phys.* **2016**, *94*, 035418.
(31) García de Abajo, F. J. Optical excitations in electron microscopy. *Rev. Mod. Phys.* **2010**, *82*, 209−275.
(32) Ishi, K.; Shibata, Y.; Takahashi, T.; Hasebe, S.; Ikezawa, M.; Takami, K.; Matsuyama, T.; Kobayashi, K.; Fujita, Y. Observation of coherent Smith-Purcell radiation from short-bunched electrons. *Phys. Rev. E: Stat. Phys., Plasmas, Fluids, Relat. Interdiscip. Top.* **1995**, *51*, R5212−R5215.
(33) Geim, A. K.; Novoselov, K. S. The rise of graphene. *Nat. Mater.* **2007**, *6*, 183.
(34) Koppens, F. H.; Chang, D. E.; Garcia de Abajo, F. J. Graphene plasmonics: a platform for strong light−matter interactions. *Nano Lett.* **2011**, *11*, 3370.
(35) Bao, Q.; Loh, K. P. Graphene photonics, plasmonics, and broadband optoelectronic devices. *ACS Nano* **2012**, *6*, 3677.
(36) Chen, J.; Badioli, M.; Alonso-González, P.; Thongrattanasiri, S.; Huth, F.; Osmond, J.; Spasenović, M.; Centeno, A.; Pesquera, A.; Godignon, P.; et al. Optical nano-imaging of gate-tunable graphene plasmons. *Nature* **2012**, *487*, 77.
(37) Ju, L.; Geng, B.; Horng, J.; Girit, C.; Martin, M.; Hao, Z.; Bechtel, H. A.; Liang, X.; Zettl, A.; Shen, Y. R.; Wang, F. Graphene plasmonics for tunable terahertz metamaterials. *Nat. Nanotechnol.* **2011**, *6*, 630.
(38) Fan, Y.; Shen, N. H.; Koschny, T.; Soukoulis, C. M. Tunable terahertz meta-surface with graphene cut-wires. *ACS Photonics* **2015**, *2*, 151.
(39) Lee, S. H.; Choi, M.; Kim, T. T.; Lee, S.; Liu, M.; Yin, X.; Choi, H. K.; Lee, S. S.; Choi, C. G.; Choi, S. Y.; et al. Switching terahertz waves with gate-controlled active graphene metamaterials. *Nat. Mater.* **2012**, *11*, 936.
(40) Kim, S.; Jang, M. S.; Brar, V. W.; Tolstova, Y.; Mauser, K. W.; Atwater, H. A. Electronically tunable extraordinary optical transmission in graphene plasmonic ribbons coupled to subwavelength metallic slit arrays. *Nat. Commun.* **2016**, *7*, 12323.
(41) Pendry, J. B.; Huidobro, P. A.; Luo, Y.; Galiffi, E. Compacted dimensions and singular plasmonic surfaces. *Science* **2017**, *358*, 915.
(42) Wu, T.; Luo, Y.; Maier, S. A.; Wei, L. Phase-matching and Peak Nonlinearity Enhanced Third-Harmonic Generation in Graphene Plasmonic Coupler. *Phys. Rev. Appl.* **2019**, *11*, 014049.
(43) Li, L.; Li, T.; Wang, S. M.; Zhang, C.; Zhu, S. N. Plasmonic Airy Beam Generated by In-Plane Diffraction. *Phys. Rev. Lett.* **2011**, *107*, 126804.
(44) Li, L.; Li, T.; Wang, S. M.; Zhu, S. N. Collimated Plasmon Beam: Nondiffracting versus Linearly Focused. *Phys. Rev. Lett.* **2013**, *110*, 046807.
(45) Kraft, M.; Luo, Y.; Pendry, J. B. Transformation Optics: A Time- and Frequency-Domain Analysis of Electron-Energy Loss Spectroscopy. *Nano Lett.* **2016**, *16*, 5156−5162.
(46) Hanson, G. W. Dyadic Green's functions and guided surface waves for a surface conductivity model of graphene. *J. Appl. Phys.* **2008**, *103*, 064302.
(47) Jablan, M.; Buljan, H.; Soljačić, M. Plasmonics in graphene at infrared frequencies. *Phys. Rev. B: Condens. Matter Mater. Phys.* **2009**, *80*, 245435.
(48) Bolotin, K. I.; Sikes, K. J.; Jiang, Z.; Klima, M.; Fudenberg, G.; Hone, J.; Kim, P.; Stormer, H. L. Ultrahigh electron mobility in suspended graphene. *Solid State Commun.* **2008**, *146*, 351−355.
(49) Ni, G. X.; McLeod, A. S.; Sun, Z.; Wang, L.; Xiong, L.; Post, K. W.; Sunku, S. S.; Jiang, B. Y.; Hone, J.; Dean, C. R.; Fogler, M. M.; Basov, D. N. Fundamental limits to graphene plasmonics. *Nature* **2018**, *557*, 530−533.


DOI: 10.1021/acsphotonics.9b00251
*ACS Photonics* XXXX, XXX, XXX−XXX

(50) Low, T.; Avouris, P. Graphene plasmonics for terahertz to mid-infrared applications. *ACS Nano* **2014**, *8*, 1086.
(51) Ma, W.; Huang, Z.; Bai, X.; Zhan, P.; Liu, Y. Dual-Band Light Focusing Using Stacked Graphene Metasurfaces. *ACS Photonics* **2017**, *4*, 1770−1775.
(52) Andryieuski, A.; Lavrinenko, A. V. Graphene metamaterials based tunable terahertz absorber: effective surface conductivity approach. *Opt. Express* **2013**, *21*, 9144.
(53) Li, Z.; Yao, K.; Xia, F.; Shen, S.; Tian, J.; Liu, Y. Graphene plasmonic metasurfaces to steer infrared light. *Sci. Rep.* **2015**, *5*, 12423.
(54) Yatooshi, T.; Ishikawa, A.; Tsuruta, K. Terahertz wavefront control by tunable metasurface made of graphene ribbons. *Appl. Phys. Lett.* **2015**, *107*, 053105.
(55) Lu, F.; Liu, B.; Shen, S. Infrared Wavefront Control Based on Graphene Metasurfaces. *Adv. Opt. Mater.* **2014**, *2*, 794.
(56) Kim, T.-T.; Kim, H.; Kenney, M.; Park, H. S.; Kim, H.-D.; Min, B.; Zhang, S. Amplitude Modulation of Anomalously Refracted Terahertz Waves with Gated-Graphene Metasurfaces. *Adv. Opt. Mater.* **2018**, *6*, 1700507.
(57) Fan, Y.; Shen, N.-H.; Zhang, F.; Zhao, Q.; Wu, H.; Fu, Q.; Wei, Z.; Li, H.; Soukoulis, C. M. Graphene Plasmonics: A Platform for 2D Optics. *Adv. Opt. Mater.* **2019**, *7*, 1800537.



DOI: 10.1021/acsphotonics.9b00251
*ACS Photonics* XXXX, XXX, XXX−XXX